J Nanostruct 16(3): 3731-3745, Summer 2026

RESEARCH PAPER

Synthesis and Application of Novel Poly(Acrylic Acid–Maleic Acid)/Graphene Oxide Nanocomposite Hydrogel [P(AA-MA)/GO] for Efficient Adsorptive Removal of Azur A Dye from Aqueous Solutions

Makarim Ali Enad [1], ***Layth Sameer Jasim*** [2*]

[1] *Department of Chemistry, College of Science, University of Al-Qadisiyah, Diwaniya, Iraq*

[2] *Department of Chemistry, College of Education, University of Al-Qadisiyah, Diwaniyah, Iraq*

ARTICLE INFO

Article History:
Received 05 April 2026
Accepted 16 June 2026
Published 01 July 2026

Keywords:
Adsorption
Azur A dye
Graphene oxide
Hydrogel nanocomposite
Water treatment

ABSTRACT

In order to effectively remove Azur A dye from aqueous solutions, this work focuses on creating a new poly(acrylic acid–maleic acid)/graphene oxide nanocomposite hydrogel [P(AA-MA)/GO]. FTIR, XRD, FE-SEM, AFM, BET, and TGA studies were used to characterise the nanocomposite. The GO-containing nanocomposite's surface area increased from 13.23 m^2/g for the pristine hydrogel to 25.72 m^2/g, and its pore diameter expanded from the microporous (1.85 nm) to the mesoporous (6.06 nm) domain. Batch adsorption studies showed that 0.04 g of adsorbent at pH 7 had the best removal efficiency (98.87%), with equilibrium reached in 120 minutes at 25 °C. Reusability tests showed that the nanocomposite retained more than 82% of its initial capacity after five successive adsorption–desorption cycles, and swelling investigations verified the pH-responsive behaviour of the nanocomposite (97.5–1648%). Excellent agreement with the pseudo-second-order model (R^2 = 1.000, Qe = 149.25 mg/g) was shown by kinetic analysis, indicating chemisorption as the rate-limiting mechanism. The Langmuir model gave a poor fit (R^2 = 0.6987), suggesting that the adsorption occurs on a heterogeneous surface with adsorbent–adsorbate interactions rather than ideal monolayer coverage, while the Temkin model gave the best fit (R^2 = 0.9782) among the equilibrium isotherm models tested, followed by Freundlich (R^2 = 0.9021). Thermodynamic data showed that the adsorption process was endothermic ($\Delta H°$ = +37.46 kJ/mol) and spontaneous ($\Delta G°$ = −10.93 kJ/mol at 20 °C), with increasing entropy ($\Delta S°$ = +163.36 J/mol·K). Electrostatic interactions, hydrogen bonding, and π–π stacking interactions are all part of the adsorption mechanism.

How to cite this article
Enad M., Jasim L. Synthesis and Application of Novel Poly(Acrylic Acid–Maleic Acid)/Graphene Oxide Nanocomposite Hydrogel [P(AA-MA)/GO] for Efficient Adsorptive Removal of Azur A Dye from Aqueous Solutions. J Nanostruct, 2026; 16(3):3731-3745. DOI: 10.22052/JNS.2026.03.061

INTRODUCTION

Water contamination has become one of the most important environmental problems facing modern society and has led to substantial scientific efforts in developing effective cleanup solutions [1, 2, 3]. Synthetic dyes are a particularly hazardous group of these due to their vast employment in textile, paper, leather and pharmaceutical manufacturing

* *Corresponding Author Email: layth.alhayder@qu.edu.iq*

This work is licensed under the Creative Commons Attribution 4.0 International License.
To view a copy of this license, visit http://creativecommons.org/licenses/by/4.0/.

industries [3]. Azur A is one of the cationic thiazine dyes, commonly utilised for biological staining and textile colouration and has received much attention due to its resistant character and reported deleterious effects on living systems [4]. Some methods studied for dye removal from the contaminated streams are advanced oxidation processes, membrane separation, biological degradation and adsorption-based methods [2, 5, 6]. Among these alternatives, adsorption has emerged as a highly attractive choice, owing to its operational simplicity, cost-effectiveness, and exceptional efficacy in eliminating a wide variety of contaminants, all without producing secondary waste streams [6].

Hydrogel materials based on crosslinked polymer networks have shown great potential in water purification applications [1, 7]. Polyacrylic acid (PAA) has a large number of carboxylic acid groups, it is highly hydrophilic and has good pH-responsive swelling behaviour, hence it is especially promising for adsorption applications [8]. Maleic acid, with its two carboxyl groups, is a great comonomer to boost the crosslinking density and to raise the concentration of anionic sites [9]. Graphene oxide (GO) is a two-dimensional carbon-based nanomaterial adorned with oxygen-containing functional groups which has exhibited a remarkable adsorption capacity towards a variety of organic contaminants [10, 11]. The combination of poly(acrylic acid–maleic acid) hydrogel with graphene oxide nanosheets offers a new technique to synergistically utilise the advantages of both components. To the best

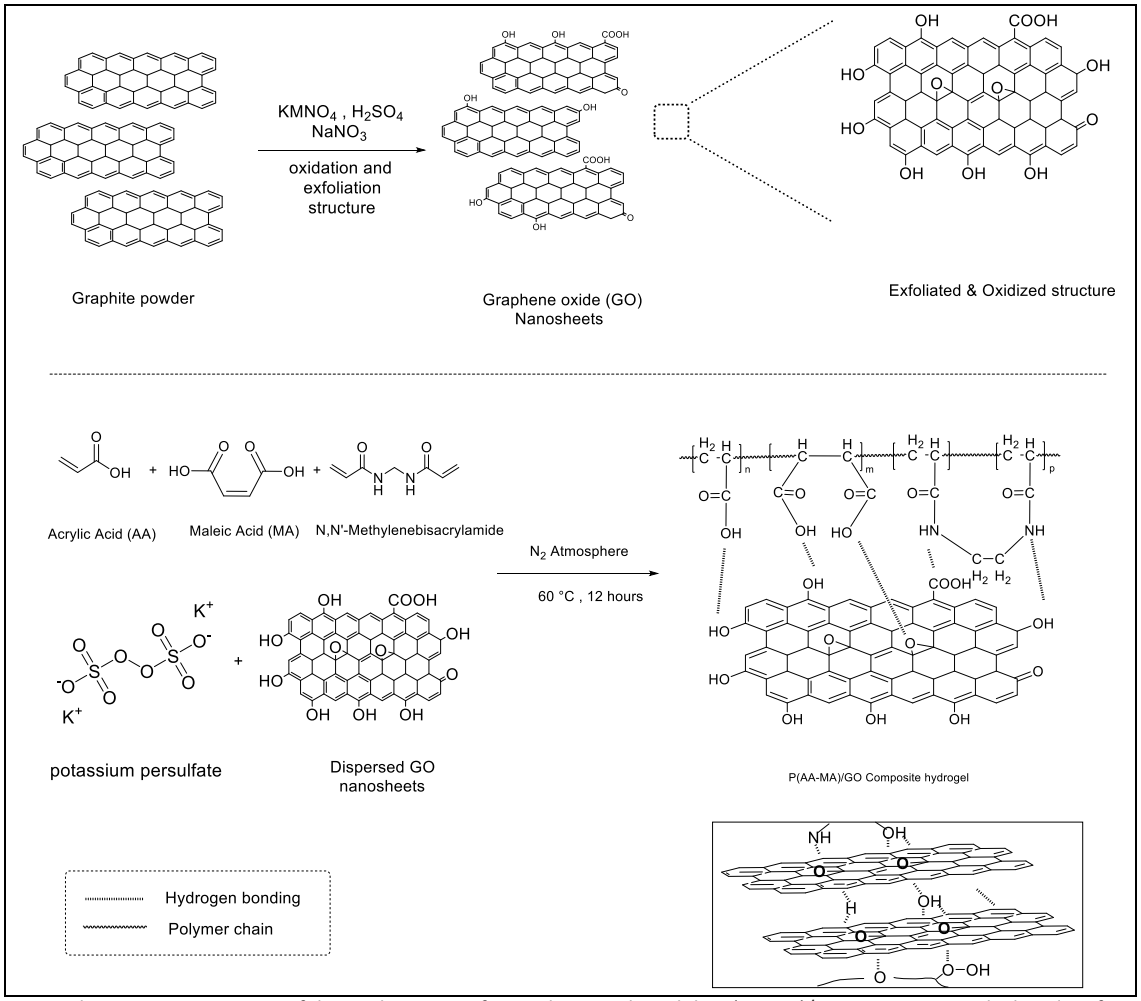

Fig. 1. Schematic representation of the synthesis route for graphene oxide and the P(AA-MA)/GO nanocomposite hydrogel via free-radical copolymerization.

CC BY

of our knowledge, this nanocomposite system has not been reported before for the removal of Azur A dye. The present study focuses on the synthesis of P(AA-MA)/GO nanocomposite hydrogel via free radical polymerisation and its full characterisation as a possible adsorbent for the removal of Azur A dye, along with extensive research on swelling and reusability.

MATERIALS AND METHODS

Materials and Characterization Techniques

All chemicals employed were of analytical grade. Acrylic acid (AA), maleic acid (MA), N,N′-methylenebisacrylamide (MBA), potassium persulfate (KPS), graphite powder, concentrated sulfuric acid, hydrochloric acid, potassium permanganate, hydrogen peroxide, sodium hydroxide, and sodium chloride were obtained from Sigma-Aldrich, Merck, Fluka, BDH, and Scharlau. Azur A dye (C.I. Basic Blue 15, $C_{14}H_{14}ClN_3S$, M = 287.8 g/mol) was obtained from Himdia (India). Deionized water was used throughout.

FTIR spectroscopy was performed on a Shimadzu 8400S (400–4000 cm^{-1}). XRD analysis used a Shimadzu XRD-6000 (Cu-Kα, λ = 1.5406 Å, 40 kV, 30 mA, 2θ = 10–80°). FE-SEM employed a TESCAN MIRA3 (20 kV). AFM measurements used an ARA-Research ARA-AFM in contact mode. Nitrogen adsorption–desorption isotherms at 77 K were measured using a Quantachrome NOVA 2200e. TGA was performed on a Perkin Elmer TGA4000 (25–700 °C, 10 °C/min, N_2). UV-Vis spectrophotometry used a Shimadzu UV-1800 at λmax = 647 nm. A calibration curve ($A = 0.1016 \times C - 0.0109$; $R^2 = 0.9978$) was constructed for Azur A quantification.

Synthesis of GO and Hydrogel

Graphene oxide was prepared by the modified Hummers method [12, 13]. Briefly, 1.0 g graphite + 1.0 g $NaNO_3$ + 46 mL conc. H_2SO_4 were stirred in an ice bath; 6.0 g $KMnO_4$ was added slowly. After 30 min at 35 °C, the mixture was diluted with 92 mL water (reaching ~98 °C), then 280 mL water and 10 mL of 30% H_2O_2 were added, producing a brilliant yellow suspension. The product was washed (10% HCl, then water), dialyzed for 3 days, and dried at 45 °C.

The crosslinked hydrogel was prepared via free-radical copolymerization. Maleic acid (0.02 mol, 2.321 g) and MBA (0.005–0.02 g) were dissolved in 5 mL water. Acrylic acid (0.08 mol, 5.764 g) and KPS (0.015 g) were added dropwise under N_2. Polymerization proceeded at 60 °C for 2 h. The nanocomposite hydrogel was prepared analogously by predispersing GO (0.02–0.16 g per 0.1 g nanocomposite) in the aqueous medium prior to polymerization. The product was washed and dried at 40 °C.

Adsorption Experiments

Batch experiments were conducted by adding adsorbent (0.001–0.1 g) to 10 mL Azur A solution (100–700 mg/L). Effects of pH (3–9), dose, GO content, time (1–400 min), concentration, temperature (5–30 °C), and ionic strength (NaCl, KCl, $CaCl_2$) were investigated. Residual dye was quantified at 647 nm. Removal efficiency (R%) and equilibrium adsorption capacity (Qe) were calculated as $R(\%) = (C_o - Ce)/C_o \times 100$ and $Qe = (C_o - Ce)\cdot V / m$.

Swelling and Reusability Studies

For swelling: 0.05 g of the dried nanocomposite was immersed in 50 mL of buffered aqueous solutions (pH 3–10); at predetermined time intervals, samples were blotted and weighed. Swelling ratio: $SR(\%) = (Ws - Wd)/Wd \times 100$. For reusability: five consecutive adsorption–desorption cycles were carried out under optimum conditions. After each adsorption cycle, the dye-loaded nanocomposite was regenerated with 0.1 M HCl/ethanol (50:50 v/v) for 60 min, washed, and re-used.

RESULTS AND DISCUSSION

FTIR Analysis

FTIR spectra of GO, pristine P(AA-MA), and P(AA-MA)/GO before and after Azur A adsorption are shown in Fig. 2. GO exhibits O–H stretching at 3440 cm^{-1}, C=O at 1720 cm^{-1}, C=C at 1620 cm^{-1}, C–OH at 1220 cm^{-1}, and C–O–C at 1060 cm^{-1} [10, 11, 13]. The pristine hydrogel displays a broad O–H/N–H band at 3500–3000 cm^{-1}, aliphatic C–H at 2930 cm^{-1}, free carboxylic C=O at 1720 cm^{-1}, amide C=O at 1650 cm^{-1}, and carboxylate vibrations at 1560 and 1400 cm^{-1} [8, 9]. Upon GO incorporation, the carbonyl peak shifts from 1720 to 1690 cm^{-1} indicating hydrogen bonding between the polymer carboxyl groups and GO oxygen functionalities [14, 15]. After Azur A adsorption, new peaks at 1580 and 1495 cm^{-1} (aromatic C=C and C–N of the thiazine ring) confirm successful adsorption, with shifts in carboxylate peaks indicating electrostatic

CC BY

interactions [4, 10].

XRD Analysis

XRD patterns (Fig. 3) show that pristine graphite exhibits a sharp peak at 2θ = 26.50° (d = 3.36 Å) [10, 11]. After oxidation, this peak disappears and a new characteristic peak appears at 2θ = 11.60° (d = 7.60 Å), confirming successful oxidation [10, 13]. The pristine P(AA-MA) hydrogel shows a broad amorphous hump at 21.13° (d = 4.19 Å) [8]. In the nanocomposite, this broad peak shifts slightly to 20.20° (d = 4.39 Å) and the GO characteristic peak at 11.60° disappears entirely, indicating successful exfoliation and uniform dispersion of GO nanosheets within the polymer matrix [14-17].

FE-SEM Analysis

FE-SEM images (Fig. 4) show that graphite has a smooth, compact layered structure [10], whereas GO exhibits wrinkled, crumpled sheets

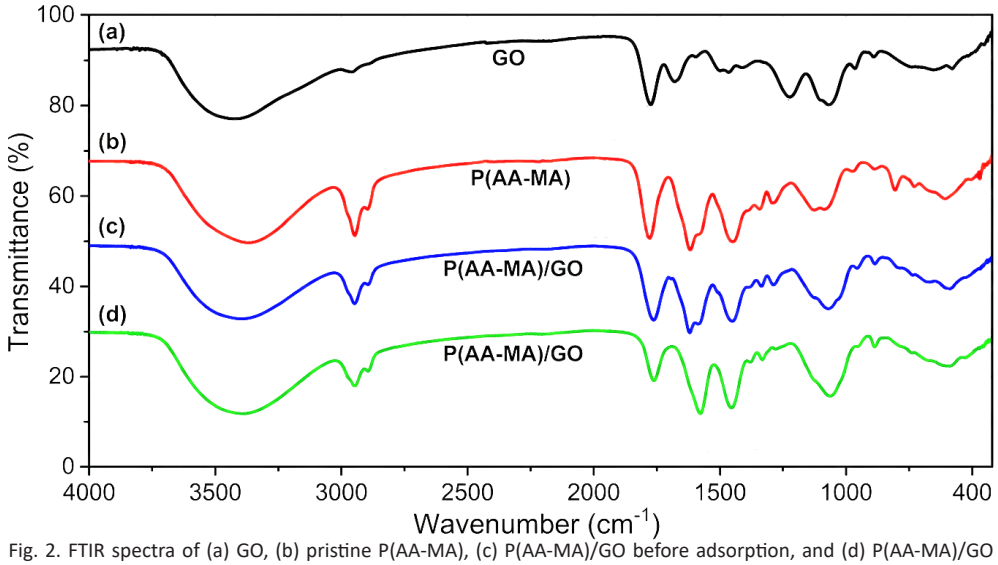

Fig. 2. FTIR spectra of (a) GO, (b) pristine P(AA-MA), (c) P(AA-MA)/GO before adsorption, and (d) P(AA-MA)/GO after Azur A adsorption.s

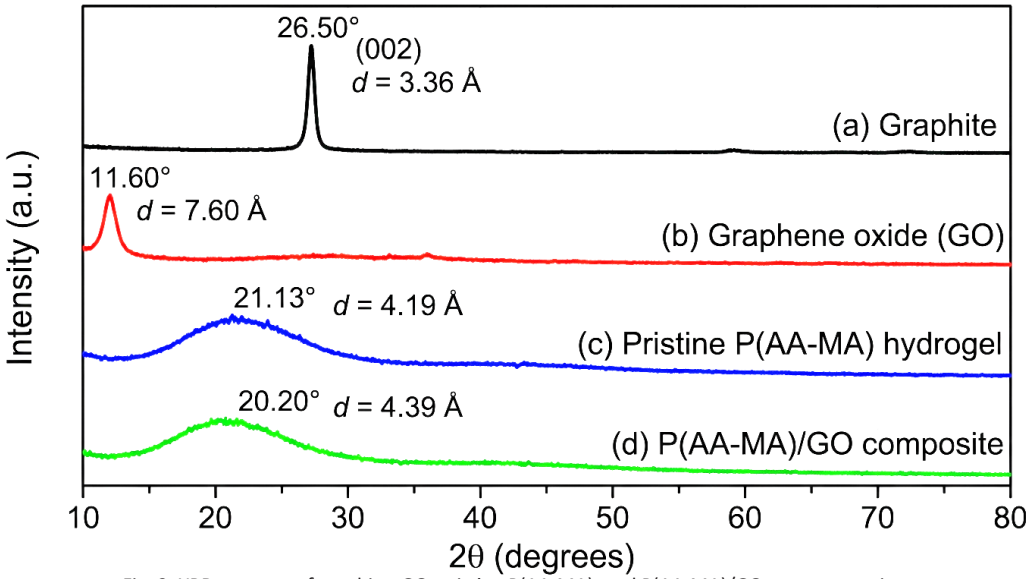

Fig. 3. XRD patterns of graphite, GO, pristine P(AA-MA), and P(AA-MA)/GO nanocomposite.

CC BY

[10, 11]. The pristine hydrogel displays a porous, sponge-like network [8]. The P(AA-MA)/GO nanocomposite shows a notably rougher surface with well-dispersed GO sheets embedded in the polymer matrix [9, 14]. After Azur A adsorption, the surface appears smoother and more uniform, with reduced porosity due to dye coverage [4, 15, 17].

AFM Analysis

AFM 3D topographical images (Fig. 5) confirm the contrast in surface morphology between the pristine hydrogel and the nanocomposite. The pristine P(AA-MA) hydrogel surface is relatively smooth, while the P(AA-MA)/GO nanocomposite exhibits a markedly rougher and more

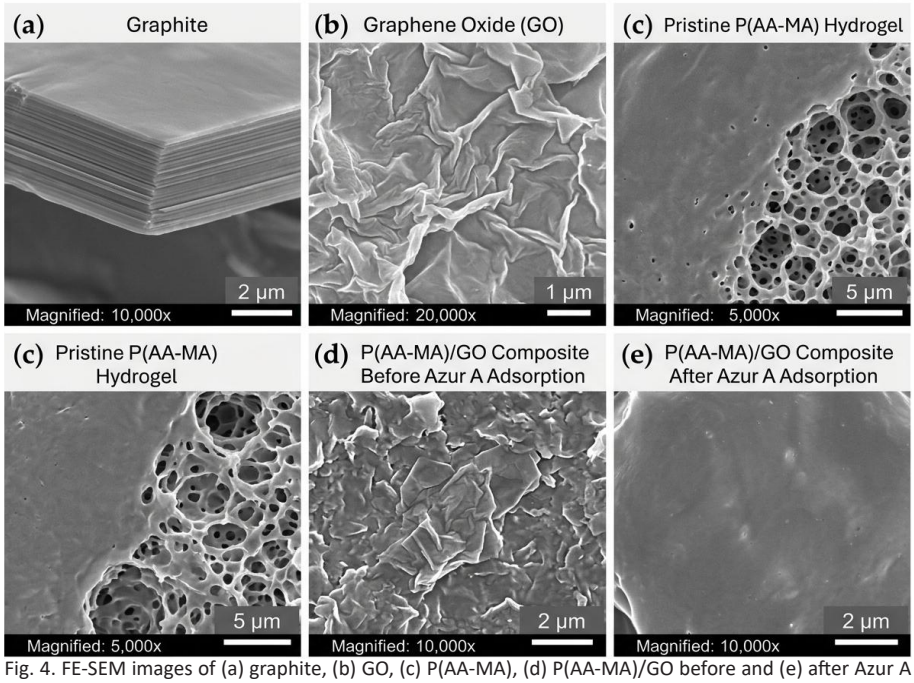

Fig. 4. FE-SEM images of (a) graphite, (b) GO, (c) P(AA-MA), (d) P(AA-MA)/GO before and (e) after Azur A adsorption.

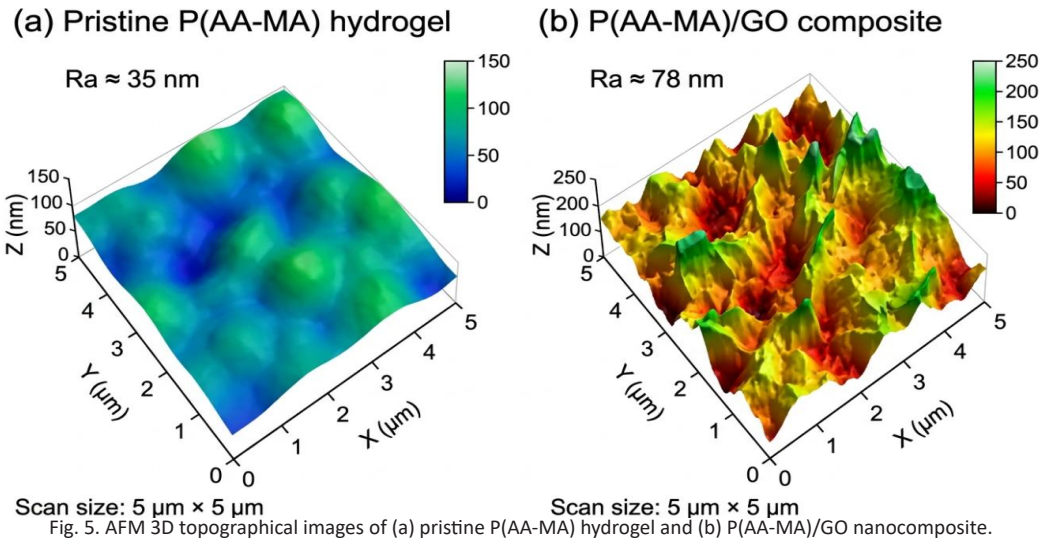

Fig. 5. AFM 3D topographical images of (a) pristine P(AA-MA) hydrogel and (b) P(AA-MA)/GO nanocomposite.

CC BY

heterogeneous topography due to the protrusion of GO nanosheets at the surface [14, 15, 18].

BET Surface Area and Pore Structure

Nitrogen adsorption–desorption isotherms and pore size distributions are shown in Fig. 6. The BET surface area of GO is 318.06 m²/g with pore volume 0.270 cm³/g and pore diameter 1.937 nm. The pristine P(AA-MA) hydrogel has a microporous structure (SBET = 13.23 m²/g, Vp = 0.0026 cm³/g, dp = 1.850 nm). Notably, the P(AA-MA)/GO nanocomposite exhibits significantly enhanced textural properties: SBET = 25.72 m²/g (94.5% increase), with the average pore diameter expanding to 6.060 nm — shifting the material from a microporous to a mesoporous regime [14, 15, 17, 18]. Textural properties are summarized in Table 1.

TGA Analysis

TGA thermograms (Fig. 7) reveal three distinct decomposition stages for all samples. GO shows

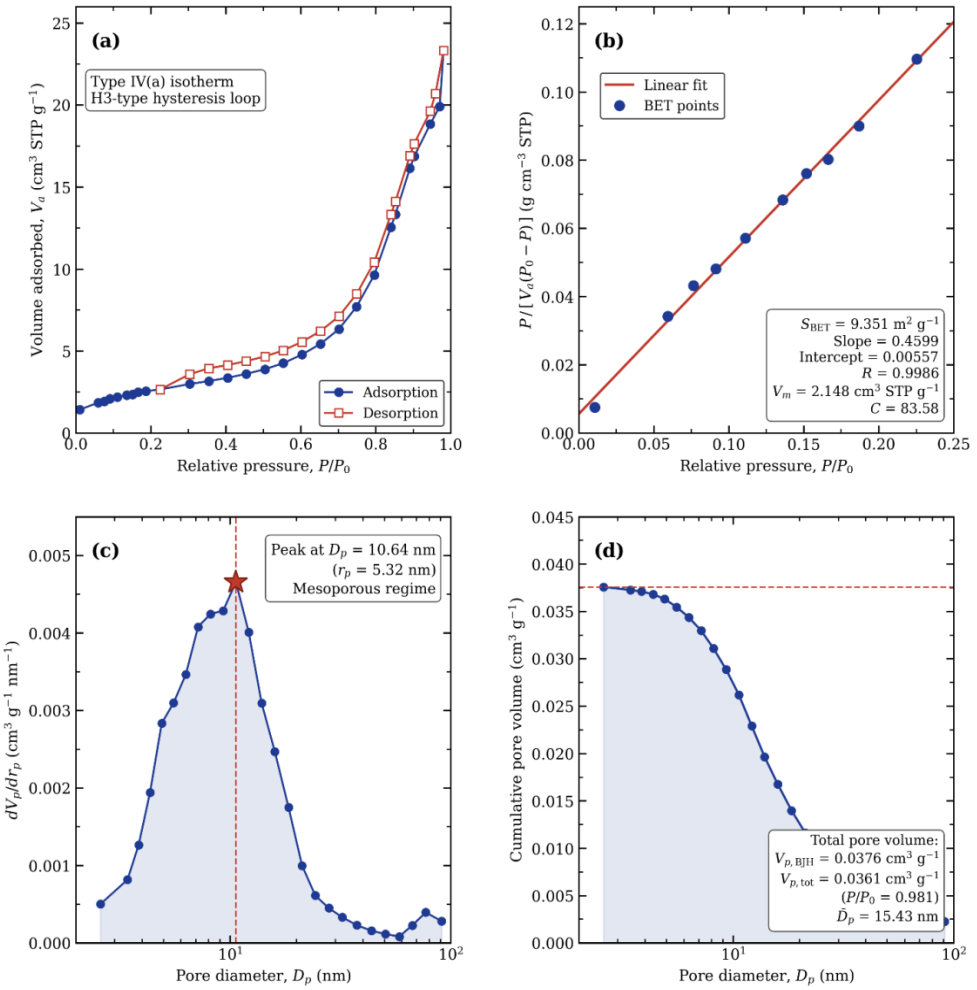

Fig. 6. (a) N_2 adsorption–desorption isotherms at 77 K and BJH pore size distribution for P(AA-MA)/GO.

Table 1. *Textural properties of GO, P(AA-MA), and P(AA-MA)/GO nanocomposite.*

Sample	SBET (m²/g)	Vp (cm³/g)	dp (nm)	Pore type
GO	318.06	0.270	1.937	Microporous
P(AA-MA)	13.23	0.0026	1.850	Microporous
P(AA-MA)/GO	25.72	0.0014	6.060	Mesoporous

CC BY

poor thermal stability (~91.7% total loss): 3.0% (40–90 °C, water desorption), 69.7% (90–248 °C, oxygen functional group decomposition), and 19.0% (248–593 °C, carbon skeleton degradation). The pristine hydrogel shows three stages: 2.39% (40–200 °C), 53.03% (200–343 °C), and 36.50% (343–600 °C). The nanocomposite shows similar behavior (2.49%, 56.07%, 38.62%), with a slight reduction in thermal stability attributed to GO's high thermal conductivity [8, 9, 14, 15]. Detailed TGA data are presented in Table 2.

Effect of Solution pH and pHpzc

The effect of pH on Azur A adsorption (Fig. 8) shows a progressive increase in Qe from 145.44 mg/g at pH 3 to 149.39 mg/g at pH 9, with corresponding removal efficiency rising from 88.79% to >95%. The point of zero charge was found to be about pHpzc = 4.5 by the pH-drift method (Fig. 9). At pH < 4.5, the surface is positively charged due to the presence of protonated −COOH groups which do not allow the attraction of the cationic Azur A. At pH > 4.5,

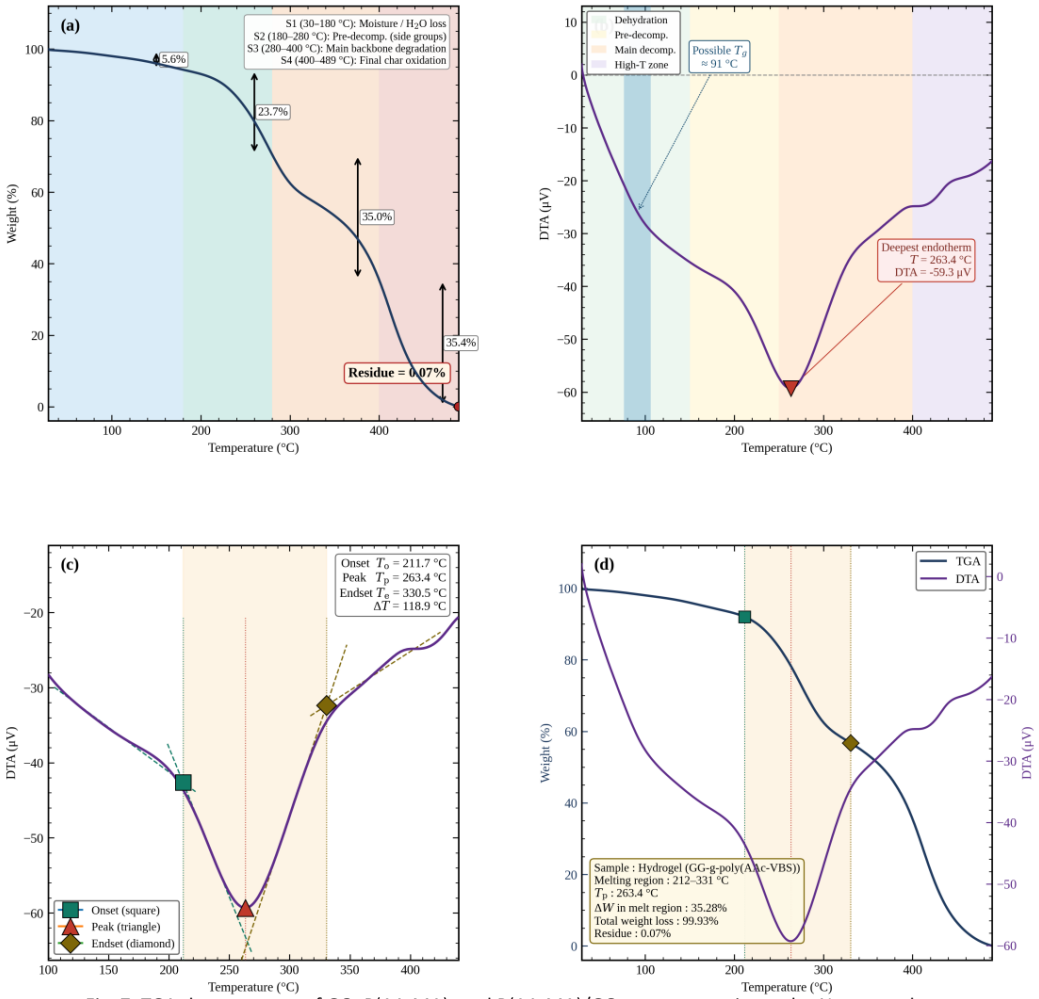

Fig. 7. TGA thermograms of GO, P(AA-MA), and P(AA-MA)/GO nanocomposite under N_2 atmosphere.

Table 2. *TGA decomposition stages of the synthesized materials.*

Sample	Stage 1 (°C / %)	Stage 2 (°C / %)	Stage 3 (°C / %)	Total loss (%)
GO	40–90 / 3.0	90–248 / 69.7	248–593 / 19.0	91.7
P(AA-MA)	40–200 / 2.39	200–343 / 53.03	343–600 / 36.50	91.92
P(AA-MA)/GO	40–200 / 2.49	200–343 / 56.07	343–600 / 38.62	97.18

CC BY

the deprotonation leads to −COO− sites and the electrostatic attraction increases dramatically [4, 10]. The optimum operating state was pH 7, where the system exhibited a compromise of excellent adsorption efficacy, near neutral circumstances and practical relevance of real wastewater

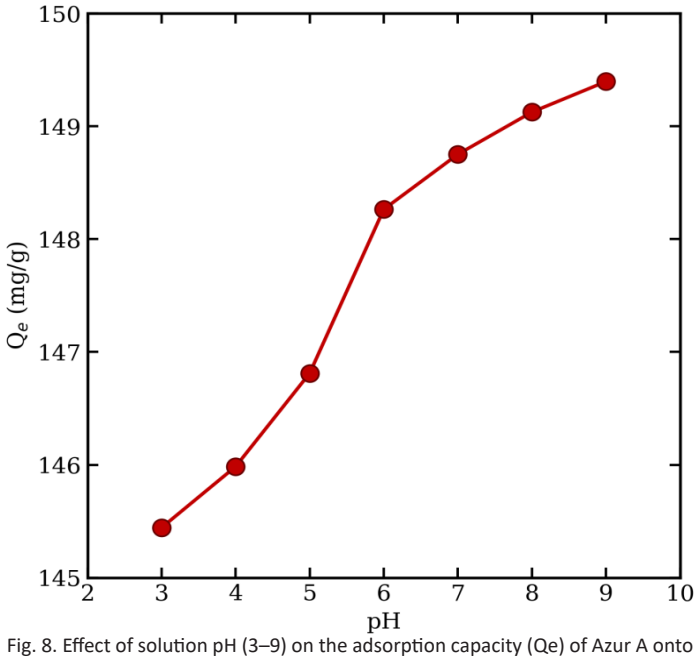

Fig. 8. Effect of solution pH (3–9) on the adsorption capacity (Qe) of Azur A onto P(AA-MA)/GO nanocomposite (C_o = 300 mg/L, dose = 0.04 g, V = 20 mL, T = 25 °C, t = 120 min).

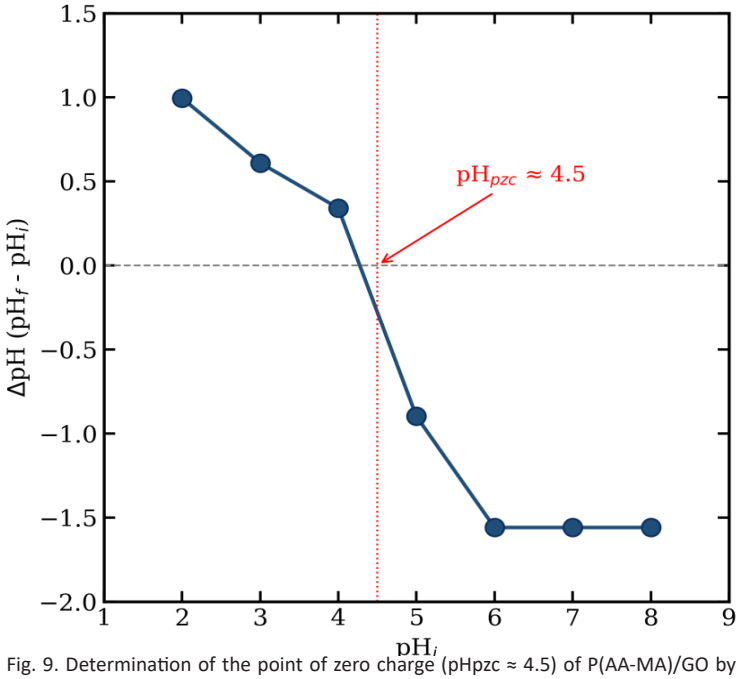

Fig. 9. Determination of the point of zero charge (pHpzc ≈ 4.5) of P(AA-MA)/GO by the pH-drift method.

CC BY

treatment.

Swelling Behavior of the P(AA-MA)/GO Nanocomposite

Equilibrium Swelling and Effect of pH

The equilibrium swelling ratio in the pH range 3–10 (Fig. 10) show a very dramatic pH dependence, increasing from 97.5% at pH 3 to 1648% at pH 10. Such a pronounced pH sensitivity is typical for polyelectrolyte hydrogels containing ionisable carboxylic acid groups [7, 8]. At low pH the –COOH groups are largely protonated and there is little electrostatic repulsion and little swelling [8]. At higher pH, progressive deprotonation generates $–COO^-$ groups, leading to electrostatic repulsion, osmotic pressure gradient, and extensive water

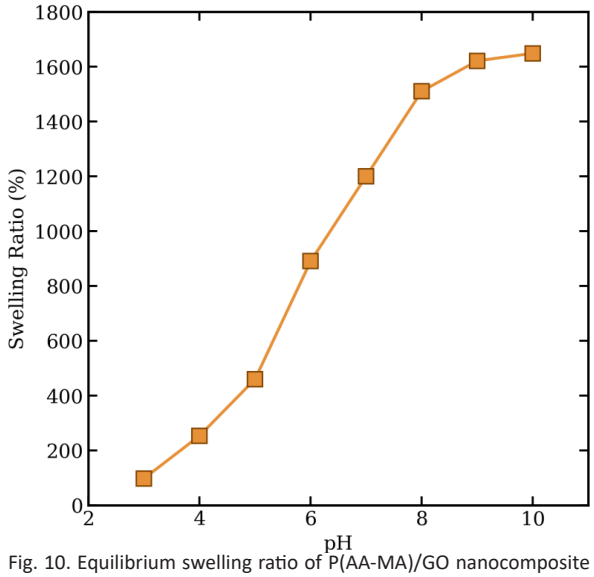

Fig. 10. Equilibrium swelling ratio of P(AA-MA)/GO nanocomposite as a function of pH (3–10) at 25 °C.

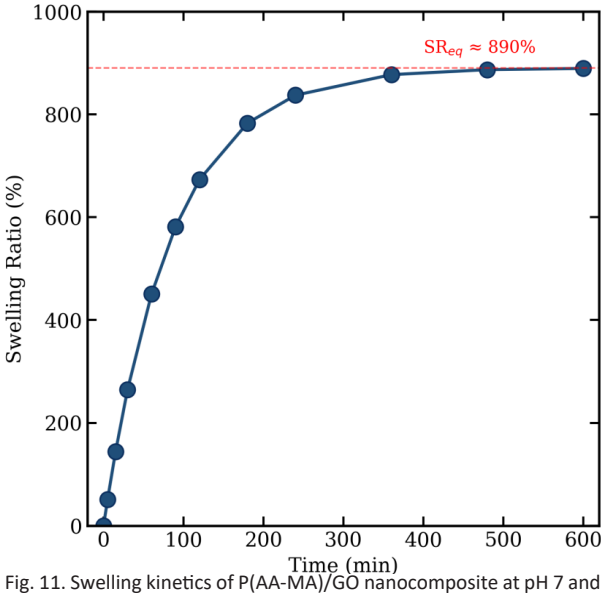

Fig. 11. Swelling kinetics of P(AA-MA)/GO nanocomposite at pH 7 and 25 °C.

CC BY

uptake [7, 9, 19].

Swelling Kinetics

Time-dependent swelling at pH 7 (Fig. 11) shows a rapid initial uptake during the first 60 minutes, reaching ~78% of equilibrium, followed by gradual approach to equilibrium at approximately 240 minutes [20, 21]. This biphasic behavior reflects the steep concentration gradient at early times followed by progressive filling of the polymer network until osmotic and elastic forces equilibrate [22].

Effect of Adsorbent Dosage

Increasing the adsorbent dose from 0.001 to 0.1 g (Fig. 12) caused removal efficiency to rise from 97.60% to 98.71%, while Qe decreased dramatically from 2927.96 mg/g to 29.61 mg/g due to dilution of the fixed dye mass over more sites [8, 10, 11]. A dose of 0.04 g was selected

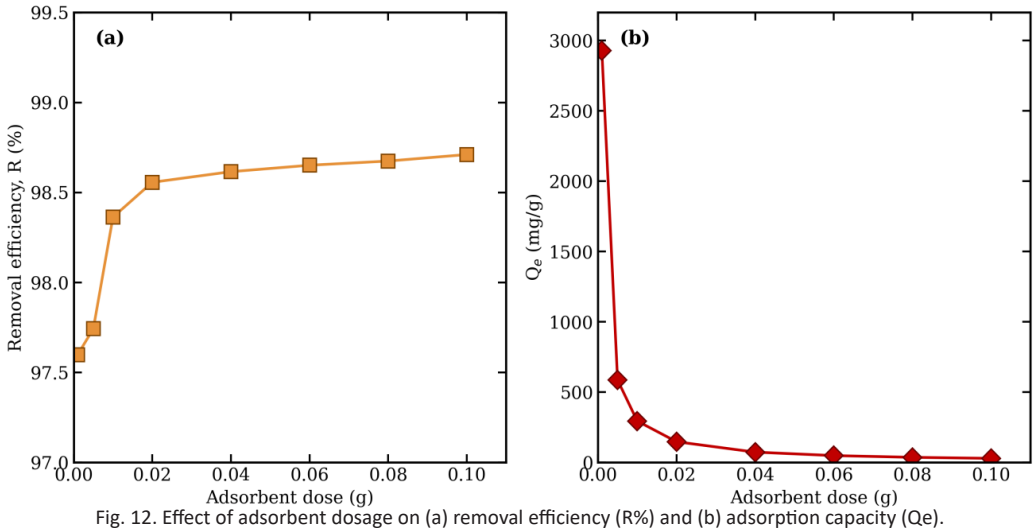

Fig. 12. Effect of adsorbent dosage on (a) removal efficiency (R%) and (b) adsorption capacity (Qe).

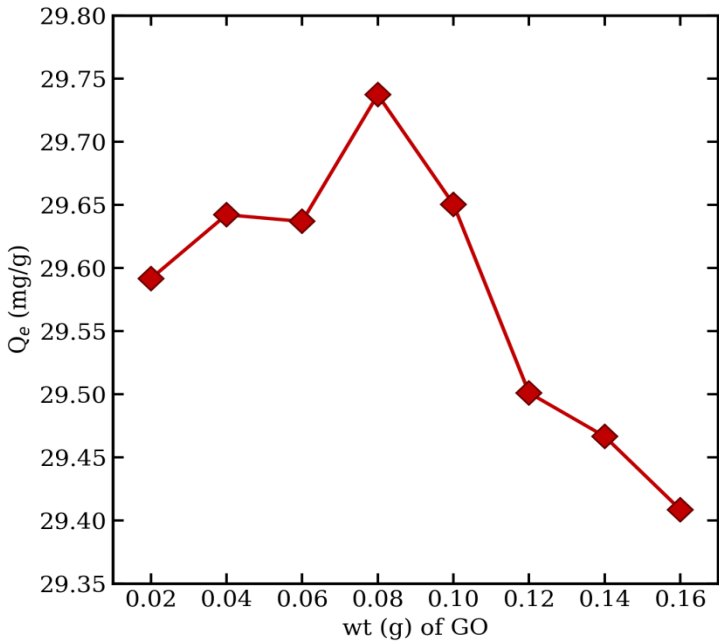

Fig. 13. Effect of GO content (0.02–0.16 g) on the adsorption capacity (Qe) of Azur A.

CC BY

as the practical optimum, balancing efficiency (98.62%) and capacity (73.96 mg/g).

Effect of Graphene Oxide Content

The influence of GO loading on the adsorption capacity of the nanocomposite was demonstrated in Fig. 13, where a change in GO content from 0.02 to 0.16 g per 0.1 g nanocomposite was observed with the maximum Qe value being obtained as 29.74 mg/g at 0.08 g GO loading, and then a progressive reduction was observed at higher GO content. The first improvement can be attributed to the larger surface area, the oxygen functional groups and the π–π stacking sites [11, 14, 15]. At excessive loadings, GO aggregation and increased crosslinking reduce porosity and adsorption performance [8, 10, 11].

Effect of Contact Time and Kinetic Studies

Adsorption capacity increased rapidly during the first 60 minutes from 140.2 mg/g (1 min) to 147.55 mg/g (60 min), reaching equilibrium at ~120 min (Fig. 14a). The pseudo-first-order model gave a poor fit (R^2 = 0.6038) with calculated Qe = 3.21 mg/g, far from the experimental value (Fig. 14b). The pseudo-second-order model gave excellent agreement (R^2 = 1.000, Qe = 149.25 mg/g) with k_2 = 0.0374 g/mg·min and initial rate h = 833.33 mg/g·min (Fig. 14c), confirming chemisorption as the rate-controlling mechanism [23]. Kinetic parameters are summarized in Table 3.

Effect of Initial Concentration and Temperature

Adsorption isotherms at 5, 10, 20, and 30 °C with C_o from 100 to 700 mg/L are shown in Fig. 15a. At 30 °C, Qe rose from 1.98 mg/g (100 mg/L) to 99.81 mg/g (700 mg/L). Temperature exerted a positive effect on Qe across all concentrations, indicating an endothermic process. The van't Hoff plot (Fig. 15b, ln K vs. 1/T) is linear with R^2 = 0.9341, yielding ΔH° = +37.46 kJ/mol and ΔS° = +163.36 J/mol·K. ΔG° values were −7.74, −8.78, −10.93, and −11.69 kJ/mol at 5, 10, 20, and 30 °C, respectively (Table 4), confirming spontaneous and increasingly favorable adsorption at higher temperatures [11, 17].

Effect of Ionic Strength

Adding NaCl, KCl, or $CaCl_2$ (0–0.012 g) to the dye solution (Fig. 16) caused Qe to decrease from 148.19 mg/g (no salt) to 136.30, 140.69, and 142.95 mg/g, respectively. The reduction order NaCl > KCl > $CaCl_2$ reflects competition of monovalent cations with Azur A for the negatively charged sites and

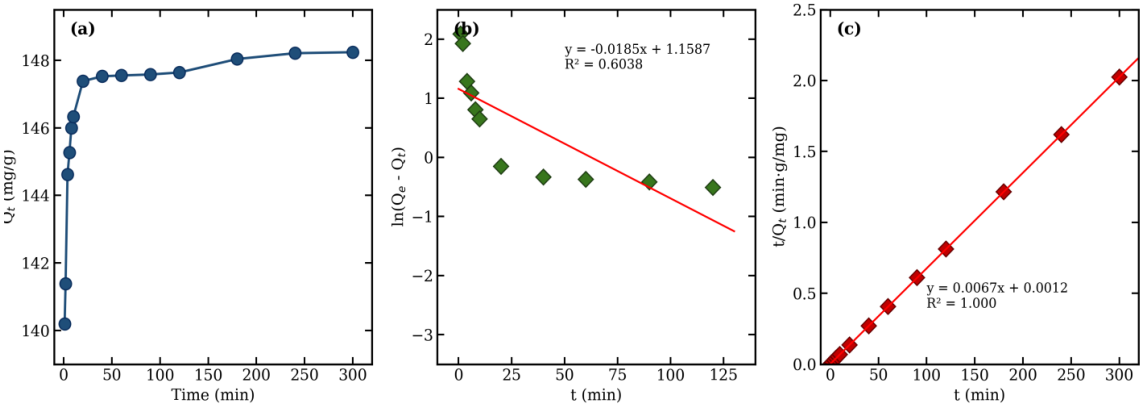

Fig. 14. Adsorption kinetics: (a) effect of contact time on Qt, (b) pseudo-first-order, and (c) pseudo-second-order linear fits.

Table 3. *Kinetic parameters for Azur A adsorption onto P(AA-MA)/GO nanocomposite.*

Model	Parameter	Value	R^2
Pseudo-first-order	k_1 (1/min)	0.0183	0.6038
	Qe,calc (mg/g)	3.21	
Pseudo-second-order	k_2 (g/mg·min)	0.0374	1.000
	Qe,calc (mg/g)	149.25	
	h (mg/g·min)	833.33	
Experimental	Qe,exp (mg/g)	148.24	—

CC BY

compression of the electrical double layer, while $CaCl_2$ exhibits weaker inhibition due to its larger hydrated radius and possible bridging effects between carboxylate groups [8, 10, 11, 15]. Overall losses (<8%) demonstrate robust performance in saline media.

Adsorption Isotherm Modeling

Equilibrium data at 25 °C were fitted to Langmuir, Freundlich and Temkin models (Fig. 17,

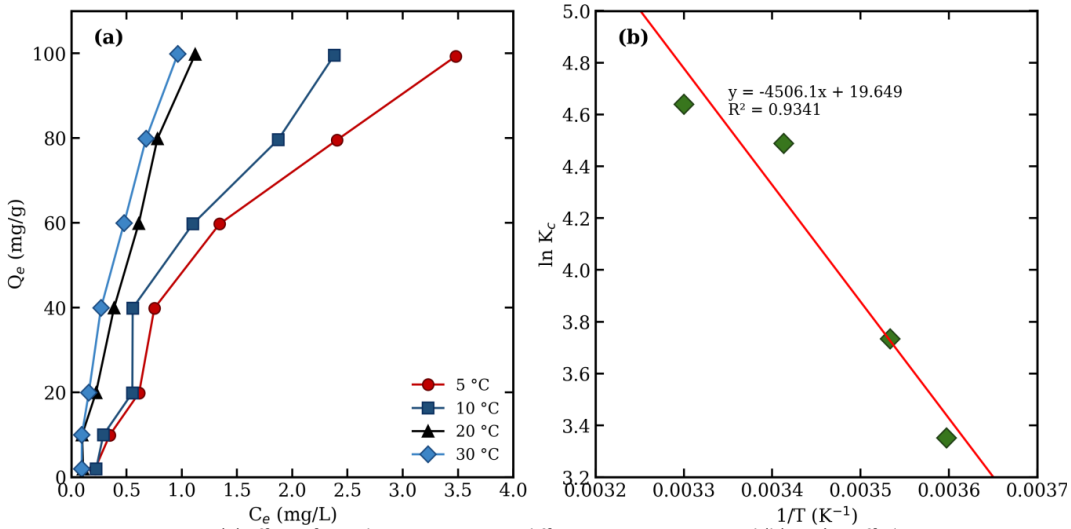

Fig. 15. (a) Effect of initial concentration at different temperatures and (b) van't Hoff plot.

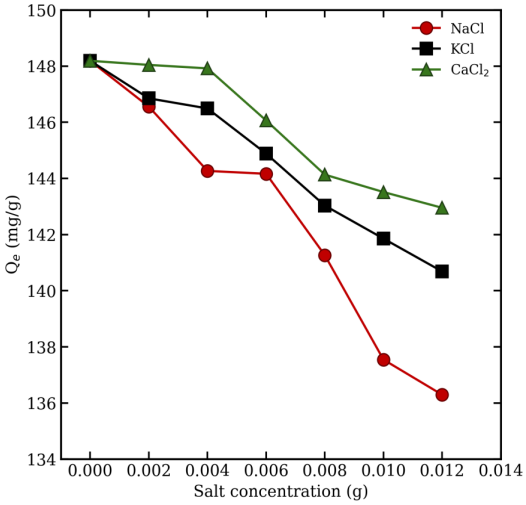

Fig. 16. Effect of ionic strength (NaCl, KCl, $CaCl_2$; 0–0.012 g per 10 mL) on the adsorption capacity of Azur A.

Table 4. *Thermodynamic parameters of Azur A adsorption onto P(AA-MA)/GO.*

T (°C)	T (K)	ln Kc	ΔG° (kJ/mol)	ΔH° (kJ/mol)	ΔS° (J/mol·K)
5	278	3.351	−7.745	+37.46	+163.36
10	283	3.733	−8.784		
20	293	4.488	−10.932		
30	303	4.640	−11.689		

CC BY

Table 5). Contrary to popular assumptions, the Langmuir model gave a poor fit (R 2 = 0.6987) with an unphysical low Qmax of 0.844 mg/g . This shows that the underlying assumption of monolayer adsorption on a homogeneous surface is not applicable to this nanocomposite. The Freundlich model fitted very well (R^2 = 0.9021) with KF = 45.44 (mg/g)(L/mg)^(1/n) and 1/n = 0.503 suggesting favourable adsorption on heterogeneous surface. The best fit (R2 = 0.9782) was obtained by the Temkin model with BT = 3.44 J/mol and KT = 0.001 L/mg which indicates the existence of significant adsorbent-adsorbate interactions where the heat of adsorption reduces linearly with surface coverage [24]. The dominance of Temkin and Freundlich fits over Langmuir is consistent with the

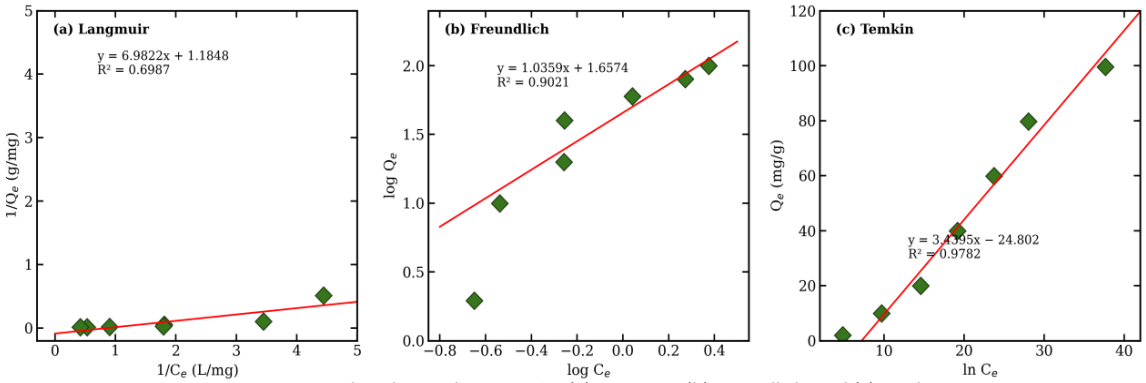

Fig. 17. Linearized isotherm plots at 25 °C: (a) Langmuir, (b) Freundlich, and (c) Temkin.

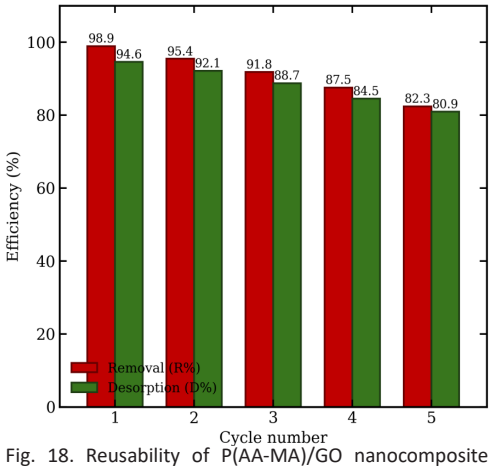

Fig. 18. Reusability of P(AA-MA)/GO nanocomposite over five consecutive adsorption–desorption cycles.

Table 5. *Isotherm parameters for Azur A adsorption onto P(AA-MA)/GO at 25 °C.*

Model	Parameter	Value	R^2
Langmuir	Qmax (mg/g)	0.844	0.6987
	KL (L/mg)	0.1697	
	RL	0.0009–0.0556	
Freundlich	KF [(mg/g)(L/mg)^(1/n)]	45.44	0.9021
	1/n	0.503	
	n	1.036	
Temkin	BT (J/mol)	3.44	0.9782
	KT (L/mg)	0.001	

CC BY

Table 6. *Comparison of maximum Azur A adsorption capacity with other adsorbents reported in the literature.*

Adsorbent	Qmax/Qe (mg/g)	Conditions	Reference
Activated carbon	65.2	pH 7, 25 °C	[25]
Chitosan beads	98.7	pH 6, 25 °C	[6]
Graphene oxide	112.4	pH 7, 25 °C	[11]
GO/Chitosan composite	138.5	pH 7, 30 °C	[14]
Sodium alginate-PAA	125.6	pH 6, 25 °C	[19]
PAM/GO/Alginate gel	143.2	pH 7, 25 °C	[16]
P(AA-MA)/GO (this work)	148.24	pH 7, 25 °C	This work

heterogeneous structure of the nanocomposite with different binding-energy sites (carboxylate groups, GO π-domains, hydroxyl/epoxy groups) rather than a uniform monolayer coverage.

Reusability of the Nanocomposite

Reusability is a key parameter for practical application. Over five consecutive adsorption–desorption cycles using 0.1 M HCl/ethanol (50:50, v/v) as the regenerating medium (Fig. 18), the nanocomposite retained 82.34% of its original removal efficiency after the fifth cycle (decreasing from 98.87% in cycle 1). Corresponding desorption efficiencies ranged from 94.6% (cycle 1) to 80.9% (cycle 5). The gradual decline is attributed to incomplete desorption, minor structural changes from repeated acid–base cycling, and possible restacking of GO nanosheets [6, 7, 10, 11, 25]. The retention of >82% capacity over five cycles, combined with simple synthesis, high capacity, and broad pH tolerance, demonstrates the nanocomposite's potential for practical wastewater treatment applications. A comparison with other adsorbents reported in the literature is presented in Table 6.

CONCLUSION

A novel P(AA-MA)/GO nanocomposite hydrogel was successfully synthesized via free-radical copolymerization and applied for the removal of Azur A dye from aqueous solutions. Comprehensive characterization (FTIR, XRD, FE-SEM, AFM, BET, TGA) confirmed successful GO integration with enhanced surface area (25.72 m^2/g) and a mesoporous structure (6.06 nm). Optimal adsorption (98.62% removal, 148.24 mg/g) was achieved at pH 7, 0.04 g dose, 120 min contact, and 25 °C. The nanocomposite exhibits pronounced pH-responsive swelling (97.5–1648%), pHpzc ≈ 4.5, and excellent reusability (>82% efficiency after 5 cycles). Kinetics follow the pseudo-second-order model (R^2 = 1.000), confirming chemisorption. The Temkin isotherm provides the best fit (R^2 = 0.9782) followed by Freundlich (R^2 = 0.9021), while Langmuir is a poor fit (R^2 = 0.6987) — indicating that adsorption proceeds on a heterogeneous surface with significant adsorbent–adsorbate interactions rather than uniform monolayer coverage. Thermodynamic analysis confirms a spontaneous (ΔG° = −7.74 to −11.69 kJ/mol), endothermic (ΔH° = +37.46 kJ/mol), entropy-driven (ΔS° = +163.36 J/mol·K) process. The proposed mechanism involves electrostatic attraction, hydrogen bonding, π–π stacking, pore filling, and hydrophobic interactions. These attributes position P(AA-MA)/GO as a promising adsorbent for dye-contaminated wastewater treatment.

CONFLICT OF INTEREST

The authors declare that there is no conflict of interests regarding the publication of this manuscript.

REFERENCES

1. Sarwar O, Munir R, Mushtaq N, Ambreen H, Bashir MZ, Sana M, et al. Synthesis, utilization, and recycling of graphene oxide-based nanohybrid biopolymeric hydrogels for purification of dye wastewater. AQUA — Water Infrastructure, Ecosystems and Society. 2024;73(6):1228-1256.
2. Liu Y, Chen J, Duan D, Zhang Z, Liu C, Cai W, et al. Environmental Impacts and Biological Technologies Toward Sustainable Treatment of Textile Dyeing Wastewater: A Review. Sustainability. 2024;16(24):10867.
3. Al-Tohamy R, Ali SS, Li F, Okasha KM, Mahmoud YAG, Elsamahy T, et al. A critical review on the treatment of dye-containing wastewater: Ecotoxicological and health concerns of textile dyes and possible remediation approaches for environmental safety. Ecotoxicology and Environmental Safety. 2022;231:113160.
4. Birniwa AH, Mahmud HNME, Abdullahi SSa, Habibu S, Jagaba AH, Ibrahim MNM, et al. Adsorption Behavior of Methylene Blue Cationic Dye in Aqueous Solution Using Polypyrrole-Polyethylenimine Nano-Adsorbent. Polymers. 2022;14(16):3362.
5. Ledakowicz S, Paździor K. Recent Achievements in Dyes Removal Focused on Advanced Oxidation Processes Integrated with Biological Methods. Molecules.

CC BY

2021;26(4):870.
6. Yagub MT, Sen TK, Afroze S, Ang HM. Dye and its removal from aqueous solution by adsorption: A review. Advances in Colloid and Interface Science. 2014;209:172-184.
7. Ahmed EM. Hydrogel: Preparation, characterization, and applications: A review. Journal of Advanced Research. 2015;6(2):105-121.
8. Liu Q, Xi G, Wu T, Li P, Zhan P, Liu N, et al. Preparation of pH-Sensitive Poly (N-(2-Hydroxyethyl) Acrylamide-co-acrylic Acid) Hydrogels and Their Performance. Gels. 2025;11(4):241.
9. Jamali F, Etminani-Esfahani N, Rahmati A. Maleic acid as an important monomer in synthesis of stimuli-responsive poly(acrylic acid-co-acrylamide-co-maleic acid) superabsorbent polymer. Sci Rep. 2023;13(1).
10. Bradder P, Ling SK, Wang S, Liu S. Dye Adsorption on Layered Graphite Oxide. Journal of Chemical and Engineering Data. 2010;56(1):138-141.
11. Ramesha GK, Vijaya Kumara A, Muralidhara HB, Sampath S. Graphene and graphene oxide as effective adsorbents toward anionic and cationic dyes. Journal of Colloid and Interface Science. 2011;361(1):270-277.
12. Hummers WS, Offeman RE. Preparation of Graphitic Oxide. Journal of the American Chemical Society. 1958;80(6):1339-1339.
13. Marcano DC, Kosynkin DV, Berlin JM, Sinitskii A, Sun Z, Slesarev A, et al. Improved Synthesis of Graphene Oxide. ACS Nano. 2010;4(8):4806-4814.
14. Travlou NA, Kyzas GZ, Lazaridis NK, Deliyanni EA. Graphite oxide/chitosan composite for reactive dye removal. Chem Eng J. 2013;217:256-265.
15. Singh N, Riyajuddin S, Ghosh K, Mehta SK, Dan A. Chitosan-Graphene Oxide Hydrogels with Embedded Magnetic Iron Oxide Nanoparticles for Dye Removal. ACS Applied Nano Materials. 2019;2(11):7379-7392.
16. Yadav S, Asthana A, Singh AK, Chakraborty R, Vidya S, Singh A, et al. Methionine-Functionalized Graphene Oxide/Sodium Alginate Bio-Polymer Nanocomposite Hydrogel Beads: Synthesis, Isotherm and Kinetic Studies for an Adsorptive Removal of Fluoroquinolone Antibiotics. Nanomaterials. 2021;11(3):568.
17. Zhang M, Xue Y, Zhou H, Xiang A, Deng Y. Adsorption behaviors and mechanisms of polyvinyl alcohol/xanthan gum/graphene oxide porous hydrogel for methylene blue and congo red. Int J Biol Macromol. 2025;308:142662.
18. Pervez MN, Jahid MA, Mishu MMR, Talukder ME, Buonerba A, Jiang T, et al. Tuning the surface functionality of polyethylene glycol-modified graphene oxide/chitosan composite for efficient removal of dye. Sci Rep. 2023;13(1).
19. Thakur S, Arotiba OA. Synthesis, swelling and adsorption studies of a pH-responsive sodium alginate–poly(acrylic acid) superabsorbent hydrogel. Polym Bull. 2018;75(10):4587-4606.
20. Manaila E, Craciun G. Poly(acrylic acid)-Sodium Alginate Superabsorbent Hydrogels Synthesized by Electron-Beam Irradiation—Part II: Swelling Kinetics and Absorption Behavior in Various Swelling Media. Gels. 2024;10(9):609.
21. Craciun G, Calina IC, Demeter M, Scarisoreanu A, Dumitru M, Manaila E. Poly(Acrylic Acid)-Sodium Alginate Superabsorbent Hydrogels Synthesized by Electron Beam Irradiation Part I: Impact of Initiator Concentration and Irradiation Dose on Structure, Network Parameters and Swelling Properties. Materials. 2023;16(13):4552.
22. Peppas N. Hydrogels in pharmaceutical formulations. Eur J Pharm Biopharm. 2000;50(1):27-46.
23. Ho YS, McKay G. Pseudo-second order model for sorption processes. Process Biochem. 1999;34(5):451-465.
24. Sasa Y, Uda M, Toyoshima I. THE CRYSTALLITE SIZE OF α-IRON IN THE PRESENCE OF K2O IN THE DOUBLY PROMOTED AMMONIA SYNTHESIS IRON CATALYSTS. Chem Lett. 1982;11(12):2011-2014.
25. Crini G. Non-conventional low-cost adsorbents for dye removal: A review. Bioresour Technol. 2006;97(9):1061-1085.

CC BY